Tertiary structure of bacterial selenocysteine tRNA

Yuzuru Itoh[1,2,3], Shun-ichi Sekine[1,2], Shiro Suetsugu[3] and Shigeyuki Yokoyama[1,2,*]

[1]Department of Biophysics and Biochemistry, Graduate School of Science, The University of Tokyo, 7-3-1 Hongo, Bunkyo-ku, Tokyo 113-0033, Japan, [2]RIKEN Systems and Structural Biology Center, 1-7-22 Suehiro-cho, Tsurumi, Yokohama 230-0045, Japan and [3]Laboratory of Membrane and Cytoskeleton Dynamics, Institute of Molecular and Cellular Biosciences, The University of Tokyo, 1-1-1 Yayoi, Bunkyo-ku, Tokyo 113-0032, Japan

ABSTRACT

Selenocysteine (Sec) is translationally incorporated into proteins in response to the UGA codon. The tRNA specific to Sec (tRNA^{Sec}) is first ligated with serine by seryl-tRNA synthetase (SerRS). In the present study, we determined the 3.1 Å crystal structure of the tRNA^{Sec} from the bacterium *Aquifex aeolicus*, in complex with the heterologous SerRS from the archaeon *Methanopyrus kandleri*. The bacterial tRNA^{Sec} assumes the L-shaped structure, from which the long extra arm protrudes. Although the D-arm conformation and the extra-arm orientation are similar to those of eukaryal/archaeal tRNA^{Sec}s, *A. aeolicus* tRNA^{Sec} has unique base triples, G14:C21:U8 and C15:G20a:G48, which occupy the positions corresponding to the U8:A14 and R15:Y48 tertiary base pairs of canonical tRNAs. *Methanopyrus kandleri* SerRS exhibited serine ligation activity toward *A. aeolicus* tRNA^{Sec} *in vitro*. The SerRS N-terminal domain interacts with the extra-arm stem and the outer corner of tRNA^{Sec}. Similar interactions exist in the reported tRNA^{Ser} and SerRS complex structure from the bacterium *Thermus thermophilus*. Although the catalytic C-terminal domain of *M. kandleri* SerRS lacks interactions with *A. aeolicus* tRNA^{Sec} in the present complex structure, the conformational flexibility of SerRS is likely to allow the CCA terminal region of tRNA^{Sec} to enter the SerRS catalytic site.

INTRODUCTION

The twenty-first amino acid, selenocysteine (Sec), contains selenium and is translationally incorporated into proteins in the three domains of life, Bacteria, Eukarya and Archaea (1). The Sec-specific tRNA (tRNA^{Sec}) is the longest tRNA, and its anticodon is complementary to the stop codon UGA (2). The secondary structures of the tRNA^{Sec} species from Bacteria and Eukarya/Archaea are different from the canonical structure, and even from each other (3–5). The sequence-based cloverleaf model of the bacterial tRNA^{Sec} secondary structure revealed that the acceptor and T arms have 8- and 5-bp stems, respectively. This '8 + 5' secondary structure differs not only from the '7 + 5' secondary structure of the canonical tRNAs, but also from the '9 + 4' secondary structure of eukaryal/archaeal tRNA^{Sec}s (Figure 1A–D). The D arm of tRNA^{Sec} has a 6-bp stem and a four-nucleotide loop, in contrast to the 3–4-bp D stem and 7–12-nucleotide D loop of the canonical tRNA. In addition, both the bacterial and eukaryal/archaeal tRNA^{Sec}s have a remarkably long extra arm, which is even longer than those of the type-2 tRNAs, such as tRNA^{Ser} and tRNA^{Leu}. The extra arms of the eukaryal/archaeal and bacterial tRNA^{Ser}s have 4–5- and 5–7-bp stems, respectively, while those of the tRNA^{Sec}s have 6–7- and 6–9-bp stems, respectively (4). In each organism, the extra arm of tRNA^{Sec} is always longer than that of tRNA^{Ser}.

Sec is synthesized on tRNA^{Sec} through multiple steps. First, tRNA^{Sec} is ligated with serine by seryl-tRNA synthetase (SerRS) (2). In Eukarya/Archaea, the Ser moiety of Ser-tRNA^{Sec} is phosphorylated by *O*-phosphoseryl-tRNA^{Sec} kinase (PSTK) and is then converted to Sec by the selenocysteine synthase SepSecS (6,7). By contrast, the bacterial selenocysteine synthase SelA directly converts the Ser moiety of Ser-tRNA^{Sec} to Sec (8). SerRS is naturally responsible for serine ligation to tRNA^{Ser}, which has the canonical '7 + 5' secondary structure and the characteristic extra arm. The crystal structure of the SerRS•tRNA^{Ser} complex from the bacterium *Thermus thermophilus* revealed that the N-terminal helical domain of SerRS recognizes the extra arm of tRNA^{Ser} (9). In addition, the long extra arm of tRNA^{Sec} is reportedly important for serine ligation by SerRS.

We previously reported the crystal structures of human tRNA^{Sec} and the archaeal tRNA^{Sec}•PSTK complex (10,11), and those of the human tRNA^{Sec}•SepSecS complex (12), mouse tRNA^{Sec} (13) and another archaeal

*To whom correspondence should be addressed. Tel: +81 45 503 9196; Fax: +81 45 503 9195; Email: yokoyama@riken.jp
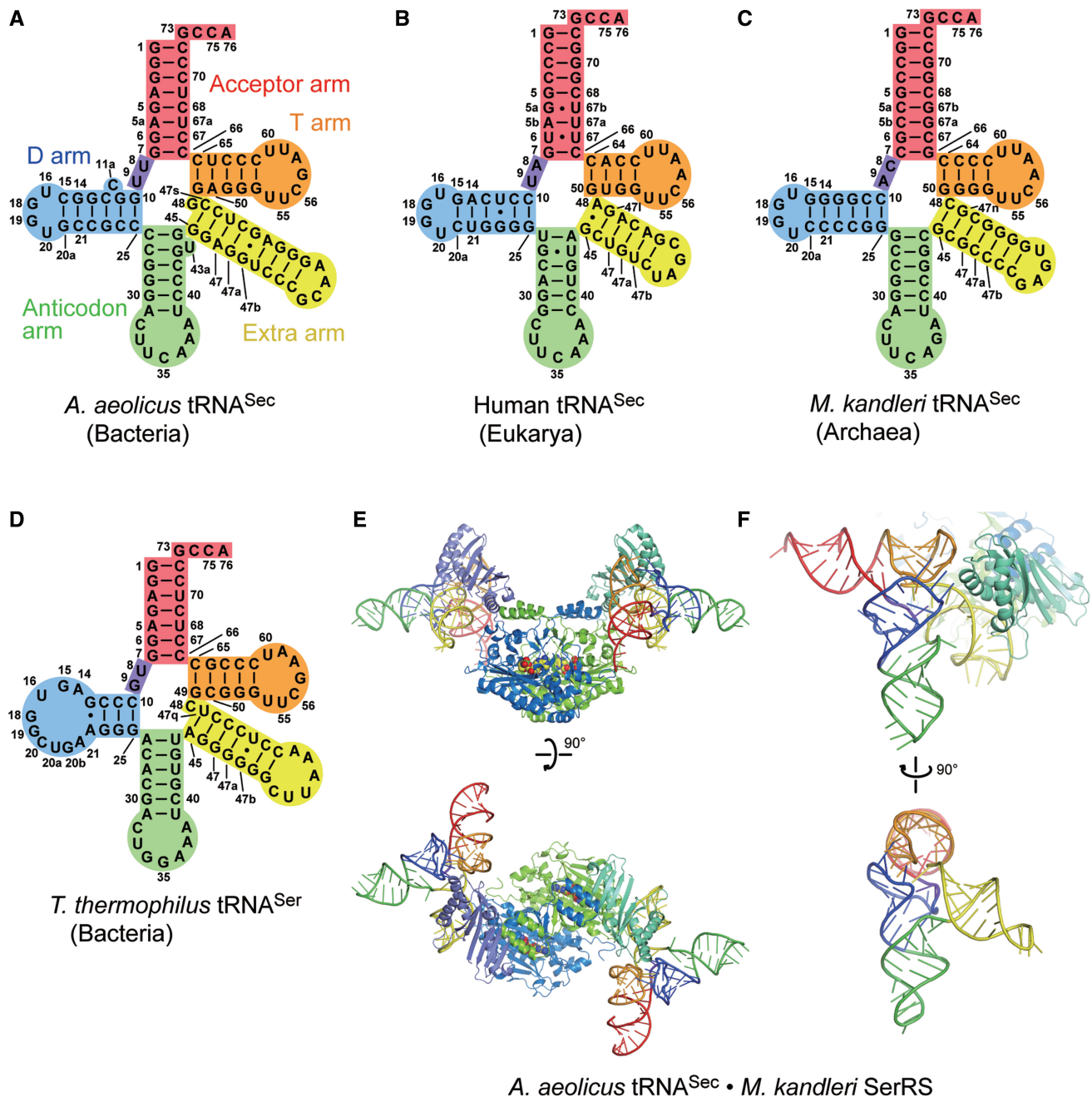
Figure 1. Overall structures. (**A–D**) The structure-based cloverleaf models of *A. aeolicus* tRNA^{Sec} (A), human tRNA^{Sec} (B), *M. kandleri* tRNA^{Sec} (C) and *T. thermophilus* tRNA^{Ser} (D). (**E** and **F**) Overall structures of *A. aeolicus* tRNA^{Sec} in complex with *M. kandleri* SerRS. *M. kandleri* SerRS and its ligand Ser-SA are shown as a ribbon diagram and a sphere model, respectively. The acceptor arm, AD linker, D arm, anticodon arm, extra arm and T arm are colored red, blue-violet, blue, lime, yellow and orange, respectively. The SerRS structure is hidden in the bottom panel of (F).

tRNA^{Sec}•PSTK complex have also been solved (14). These studies confirmed the '9 + 4' secondary structure, and revealed the characteristic features of their tertiary cores. In contrast, the bacterial tRNA^{Sec} structure, which putatively adopts the '8 + 5' secondary structure, has not been elucidated.

In this study, we solved the crystal structure of the bacterial tRNA^{Sec} from *Aquifex aeolicus*, in complex with the heterologous SerRS from the archaeon *Methanopyrus kandleri*, and confirmed the '8 + 5' secondary structure of

bacterial tRNA^{Sec}. Moreover, the tertiary core structure of the bacterial tRNA^{Sec} is distinctly different from those of its eukaryal and archaeal counterparts. On the other hand, the long extra arm of tRNA^{Sec} is recognized by *M. kandleri* SerRS in a similar manner to that of *T. thermophilus* tRNA^{Ser} by its homologous SerRS, even though the N-terminal domain of *M. kandleri* SerRS adopts a fold characteristic of the SerRSs from methanogenic archaea, and thus is distinct from those of the canonical SerRSs (15,16).

MATERIALS AND METHODS

Protein and tRNA preparation

Aquifex aeolicus tRNA^{Sec}, *M. kandleri* tRNA^{Sec} and *Archaeoglobus fulgidus* tRNA^{Cys} were prepared by *in vitro* transcription, as described (11,17,18). The *M. kandleri* SerRS gene was cloned into the pET26b vector (Novagen). The *M. kandleri* SerRS protein with 11 mutations, R55Y-E58Y-E62Y-R116Y-D118Y-E189R-D193R-E379Y-E383R-E497Y-E499Y, which targeted the protein surface to reinforce crystal packing, was used for crystallization. The native and selenomethionine (SeMet)-substituted *M. kandleri* SerRS mutant proteins were overexpressed and purified, as described (17). Furthermore, lysine methylation of SerRS was also performed to improve the crystallization efficiency (17).

Crystal structure determination

The complex of *M. kandleri* SerRS and *A. aeolicus* tRNA^{Sec} was prepared by mixing the components at final concentrations of 80 and 120 μM, respectively, in 20 mM Tris–HCl buffer (pH 7.5), containing 400 mM NaCl, 10 mM MgCl$_2$, 3 mM 2-ME and 500 μM 5′-O-[N-(L-seryl)sulfamoyl]adenosine (Ser-SA, a non-hydrolyzable analog of seryl-adenylate). Crystallization was performed at 20°C by the sitting-drop vapor diffusion method, and the phase was determined by a combination of the molecular replacement and multi-wavelength anomalous dispersion methods, using a platinum-labeled crystal (17). Labeling was performed by soaking for 10–15 h in harvest buffer containing 20 mM K$_2$Pt(CN)$_4$ (17). In the first phase determination step, we obtained the preliminary phase by molecular replacement, using the C-terminal core domain of the reported structure of *Methanosarcina barkeri* SerRS [PDB ID: 2CJ9 (19)]. The phase information was used for detecting the heavy atom sites for subsequent experimental phasing. In the later step, we placed the N-terminal domain of *M. barkeri* SerRS, based on the F_O map generated by the experimental phasing. Model building began with the modification of the placed N- and C-terminal domains (17). The final data used for structure refinement were collected from the platinum-labeled crystal, using the SerRS with 11 mutations, Lys methylation and SeMet substitution (Table 1), while the data used for phase determination were collected from a different platinum-labeled crystal without SeMet substitution (17). The structures were refined against the diffraction data with the CNS (21) and Phenix (22) programs, with iterative cycles of positional and temperature-factor refinements (Table 1). The Coot (23) and CueMol programs were used for manual fitting of the models to the electron density map.

Aminoacylation assay

The serine-ligation activities of the *A. aeolicus* and *M. kandleri* SerRSs were measured, using [^{14}C]-L-serine (Moravek). The reaction was performed at 60°C, in 50 mM Hepes-NaOH buffer (pH 7.5), containing 100 mM KCl, 20 mM MgCl$_2$, 2.0 mM dithiothreitol, 4.0 mM ATP, 0.1 mg/ml bovine serum albumin and 100 μM [^{14}C]-L-serine (5.96 GBq/mol). The time course of the reaction was monitored by removing aliquots at 1, 2 and 4 min, while the initial reaction rates to calculate the K_M and k_{cat} values were measured by removing aliquots at 30 s. The reaction was quenched by transferring each aliquot to a filter paper pre-equilibrated with 5% trichloroacetic acid (TCA), and the radioactivities of the acid-insoluble fractions were quantified by liquid scintillation counting, after the filters were washed three times with 5% ice-cold TCA and twice with 100% ethanol.

RESULTS AND DISCUSSION

Structure determination

To elucidate the tertiary structure of bacterial tRNA^{Sec}, for comparison to the eukaryal and archaeal tRNA^{Sec} species, we attempted to crystallize various bacterial
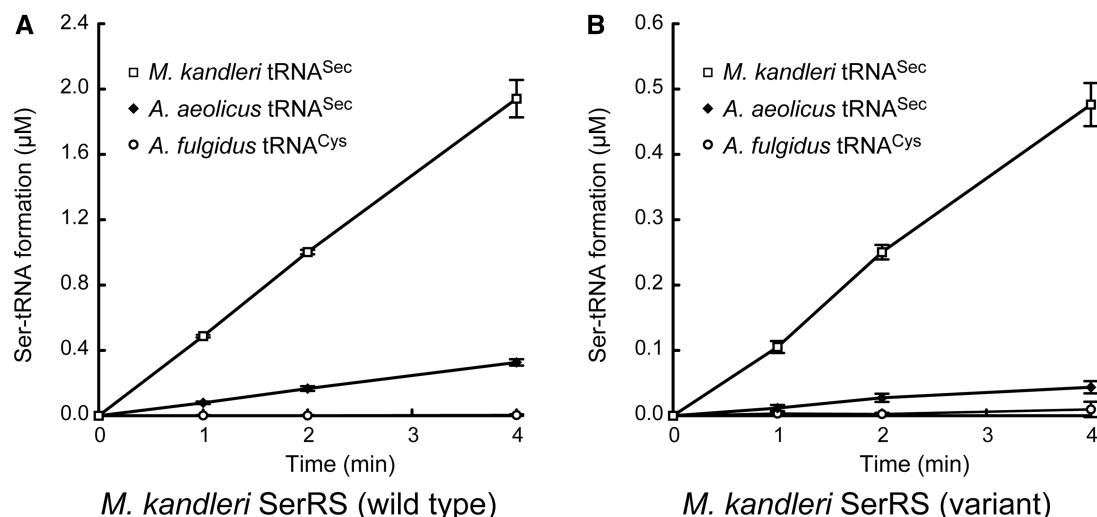
Table 1. Data collection and refinement statistics

Data collection	
Beam line	Photon Factory BL5A
Wavelength (Å)	0.97848
Space group	*I*432
Cell parameters	$a = b = c = 272.8$ Å
Resolution (Å)	50.0–3.10 (3.21–3.10)^a
Unique reflections	31 714 (3126)^a
Completeness (%)	99.9 (100.0)^a
Redundancy	15.0 (14.6)^a
R_{sym}^{b}	0.094 (0.847)^a
$I/\sigma(I)$	28.4 (3.49)^a
Structure refinement	
Working-set reflections	29 484
Test-set reflections	1556
Resolution (Å)	50.0–3.10
Number of SerRS subunits	1 (one half of dimer)
Number of RNA molecules	1
Number of protein atoms	4363
Number of RNA atoms	2090
Number of ligands	1 (Ser-SA)
Number of ions	1 (Zn^{2+}), 8 (sulfate), 15 (Pt^{2+})
Number of solvent molecules	0
R_{work}/R_{free}^{c}	0.204/0.260
Average B factor (Å^2)	
Overall	128.4
Protein	112.0
RNA	163.0
Ligand	71.4
Ion	152.2
RMSD bond lengths (Å)	0.009
RMSD bond angles (°)	1.25
Ramachandran-plot analysis^d	
Most favored regions (%)	95.2
Additional allowed regions (%)	4.8
Generously allowed regions (%)	0.0
Disallowed regions (%)	0.0

^{a}The statistics in the highest-resolution shell are given in parentheses.
^{b}$R_{sym} = \sum_{hkl}\sum_i[|I_i(hkl) - <I(hkl)>|]/\sum_{hkl}\sum_i[I_i(hkl)]$, where $I_i(hkl)$ is the intensity of the *i*th measurement of *hkl* and $<I(hkl)>$ is the average value of $I_i(hkl)$ for all *i*th measurements.
^{c}$R_{work, free} = \sum_{hkl}(||F_{obs}|-k|F_{calc}||)/\sum_{hkl}(|F_{obs}|)$, where R_{work} and R_{free} are calculated using the working-set and test-set reflections (5% of the total reflections), respectively.
^{d}Procheck (20) was used for Ramachandran-plot analysis.

Figure 2. Seine-ligation activity. Activities of 100 nM wild-type (**A**) and variant (**B**) *M. kandleri* SerRSs toward 10 μM tRNA[Sec] (*M. kandleri* or *A.aeolicus*). The variant was the SerRS with the 11 mutations, Lys methylation and SeMet subutition, used for crystallization. *A.fulgidus* tRNA[Cys] (10 μM) was used for estimating the background serine-ligation level. Each experiment was performed in quadruplicate, and the values were averaged. The error bars show standard deviations.

tRNA[Sec] species, and obtained crystals of *A.aeolicus* tRNA[Sec]. However, these crystals diffracted X-rays to only 5.5 Å resolution. Because many tRNA structures have been determined in the protein-bound forms, we tested the complex of *A. aeolicus* tRNA[Sec] with *A. aeolicus* SerRS, but the crystals still only diffracted to 8 Å resolution. On the other hand, we successfully determined the 3.1 Å resolution crystal structure of *A. aeolicus* tRNA[Sec] in its heterologous complex with *M. kandleri* SerRS (Figure 1E and F). In the process of resolution improvement, we introduced 11 mutations, R55Y-E58Y-E62Y-R116Y-D118Y-E189R-D193R-E379Y-E383R-E497Y-E499Y, methylated the lysine residues and substituted SeMet for Met, as only 5.7 Å resolution data were obtained using the wild-type SerRS without Lys methylation or SeMet substitution (17). The crystals containing the wild-type and variant SerRSs are isomorphic (17), indicating that the overall structures of tRNA[Sec] and SerRS and their contact surfaces in the crystals are the same. The mutated sites are located within non-conserved regions, but not in the tRNA[Sec] contact surface.Furthermore, the variant SerRS retained the serine-ligation activity toward the *M. kandleri* and *A. aeolicus* tRNA[Sec] s (Figure 2). The following structure descriptions are exclusively about the crystal structure using the variant SerRS, unless otherwise noted. The asymmetric unit contains one tRNA[Sec] molecule and one subunit of the SerRS homodimer. *Aquifex aeolicus* tRNA[Sec] consists 99 nucleotides (nucleotides 1–76 in Figure 1A). G73 and the 3′-CCA region in the acceptor arm are partially disordered, and the final model lacks the 3′-terminal A76.

Overall structure

The tertiary structure of *A. aeolicus* tRNA[Sec] confirmed the putative '8 + 5' secondary structure. *Aquifex aeolicus* tRNA[Sec] forms an L shape with the acceptor, T, D and anticodon arms, from which the long extra arm protrudes (Figure 3A and E). The acceptor stem consists of 8 bp, 1:72, 2:71, 3:70, 4:69, 5:68, 5a:67a, 6:67 and 7:66. The T stem includes 5 bp between nucleotides 49–53 and 61–65. The D stem is composed of 6 bp formed between nucleotides 10–15 and 25–20a, with the bulge of C11a, while the D loop has four nucleotides, 16, 18, 19 and 20 (nucleotide 17 is missing). As C26 and G44 are paired, the anticodon stem has 6 bp, from 26:44 to 31:39, with the bulge of U43a. The extra arm (nucleotides 45–47, 47a–47s and 48) of *A. aeolicus* tRNA[Sec] possesses a 9-bp stem and the linker G48. The length of the extra-arm stem (or the extra stem) varies from 6 to 9 bp among the bacterial tRNA[Sec]s (4). The extra-arm orientation is similar to those of the eukaryal/archaeal tRNA[Sec]s and even to that of tRNA[Ser] (Figure 3). In addition, tRNA[Sec] has U8 and U9 as the linker connecting the acceptor stem and the D stem ('AD linker'). The bulged nucleotides, C11a and U43a, are completely flipped out from the D and anticodon stems, respectively. In this context, bulged nucleotides are frequently observed at or near the two positions in the cloverleaf models of bacterial tRNA[Sec]s (4), and they might fine-tune the twist angles of the D and anticodon stems.

Tertiary interactions

The D-loop•T-loop interaction includes the universal G18:U55 bp, as well as the tRNA[Sec]-specific U16:U59 bp (Figure 4A) and the U20:G19:C56 base triple (Figure 6B). The interaction of U8 with C21 in the D stem forms the G14:C21:U8 base triple (Figure 4A). In the eukaryal/archaeal tRNA[Sec]s, however, the nucleotide at position 8 is not involved in the tertiary base-pairing interaction (Figure 4B and C). G48, the linker between the extra stem and the T stem, is stacked on U8, and interacts with G20a to form the unique C15:G20a:G48 base triple (Figure 4A). C15, G20a, and G48 are completely
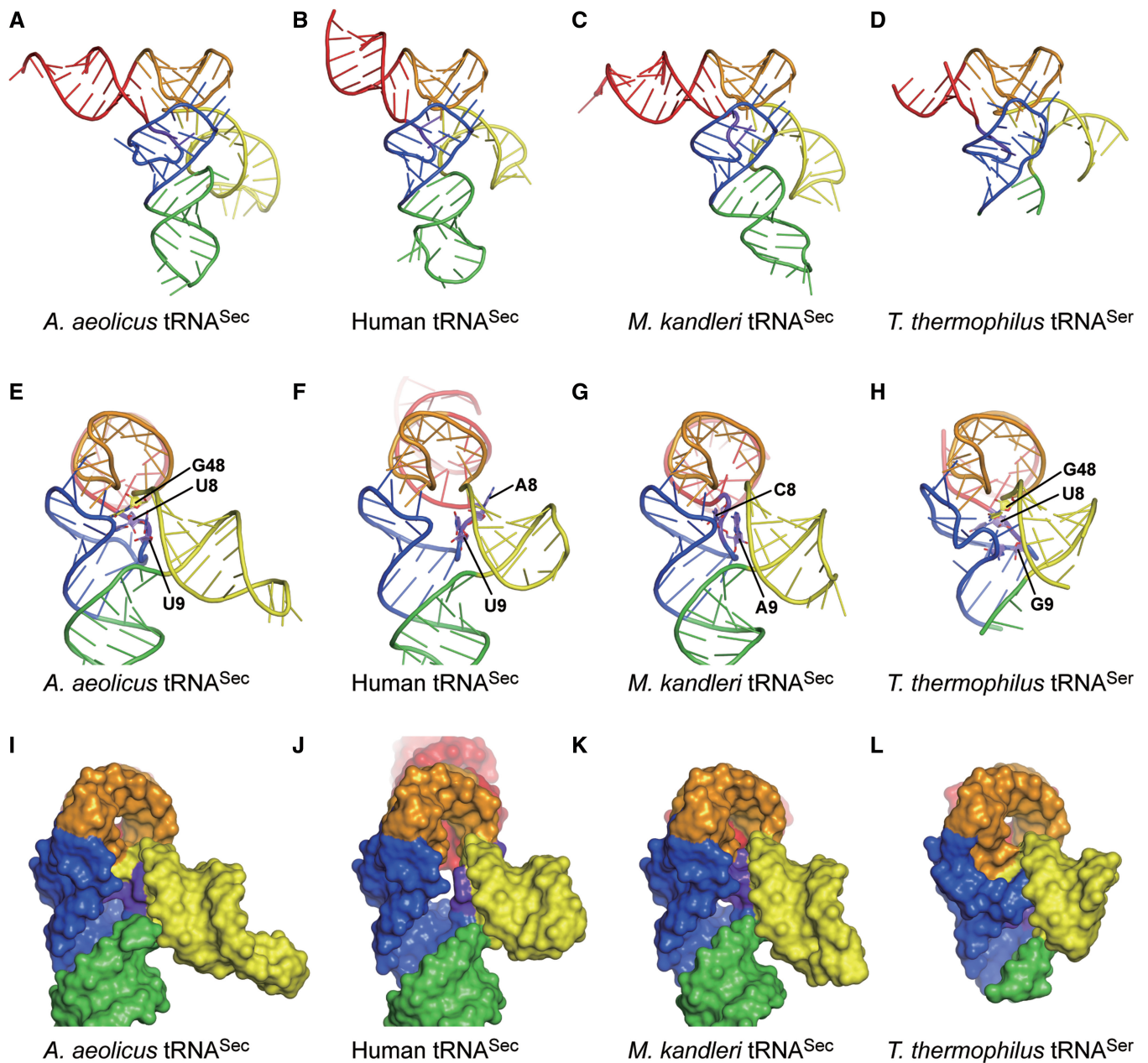
Figure 3. Structure comparisons. (**A–D**) Overall views of the present *A. aeolicus* tRNA^{Sec} (A), human tRNA^{Sec} (B) [PDB ID: 3A3A (10)], *M. kandleri* tRNA^{Sec} (C) [PDB ID: 3ADB (11)] and *T. thermophilus* tRNA^{Ser} (D) [PDB ID: 1SER (9)] structures. The structures of *M. kandleri* tRNA^{Sec} and *T. thermophilus* tRNA^{Ser} are those in their complexes with PSTK and SerRS, respectively. The ribose-phosphate backbones and the bases are shown as tubes and ladders, respectively. Each arm is indicated in the same color as in Figure 1. G73 and the terminal CCA are disordered in the human tRNA^{Sec} structure, while the distal portion of the acceptor arm, most of the anticodon arm and the extra-arm loop are disordered in the *T. thermophilus* tRNA^{Ser} structure. (**E–L**) Side views of the ladder and surface models of *A. aeolicus* tRNA^{Sec} (E and G), human tRNA^{Sec} (F and J), *M. kandleri* tRNA^{Sec} (G and K) and *T. thermophilus* tRNA^{Ser} (H and L). The linker nucleotides at positions 8, 9 and 48 are shown as plate-stick models in (E–H). The eukaryal/archaeal tRNA^{Sec}s lack the linker nucleotide corresponding to G48 in bacterial tRNA^{Sec}. The orientation of the extra arm is similar among tRNA^{Sec}s and tRNA^{Ser}.

conserved in the bacterial tRNA^{Sec}s (4). The eukaryal/archaeal tRNA^{Sec}s lack this base triple, as the extra stem is directly connected to the T stem, and there are no nucleotides corresponding to those at positions 48 and 49 (Figure 1B and C).

U9, in the AD linker, is stacked on the first base pair of the extra stem (G45:C47s) (Figure 4E). Similar base stacking of the nucleotide at position 9 is also observed

in the eukaryal/archaeal tRNA^{Sec}s (Figure 4F–I) (10,11,14). U9 of human tRNA^{Sec} is only stacked on the A48 base of the G45:A48 pair, while A9 of the archaeal tRNA^{Sec}s is stacked on the interbase hydrogen-bonding region of the base pair G45:C48. Interestingly, two distinct A9 conformations are observed in the *M. kandleri* tRNA^{Sec} molecules (chains C and D) in the complex with the PSTK dimer [PDB ID: 3ADD (11)]
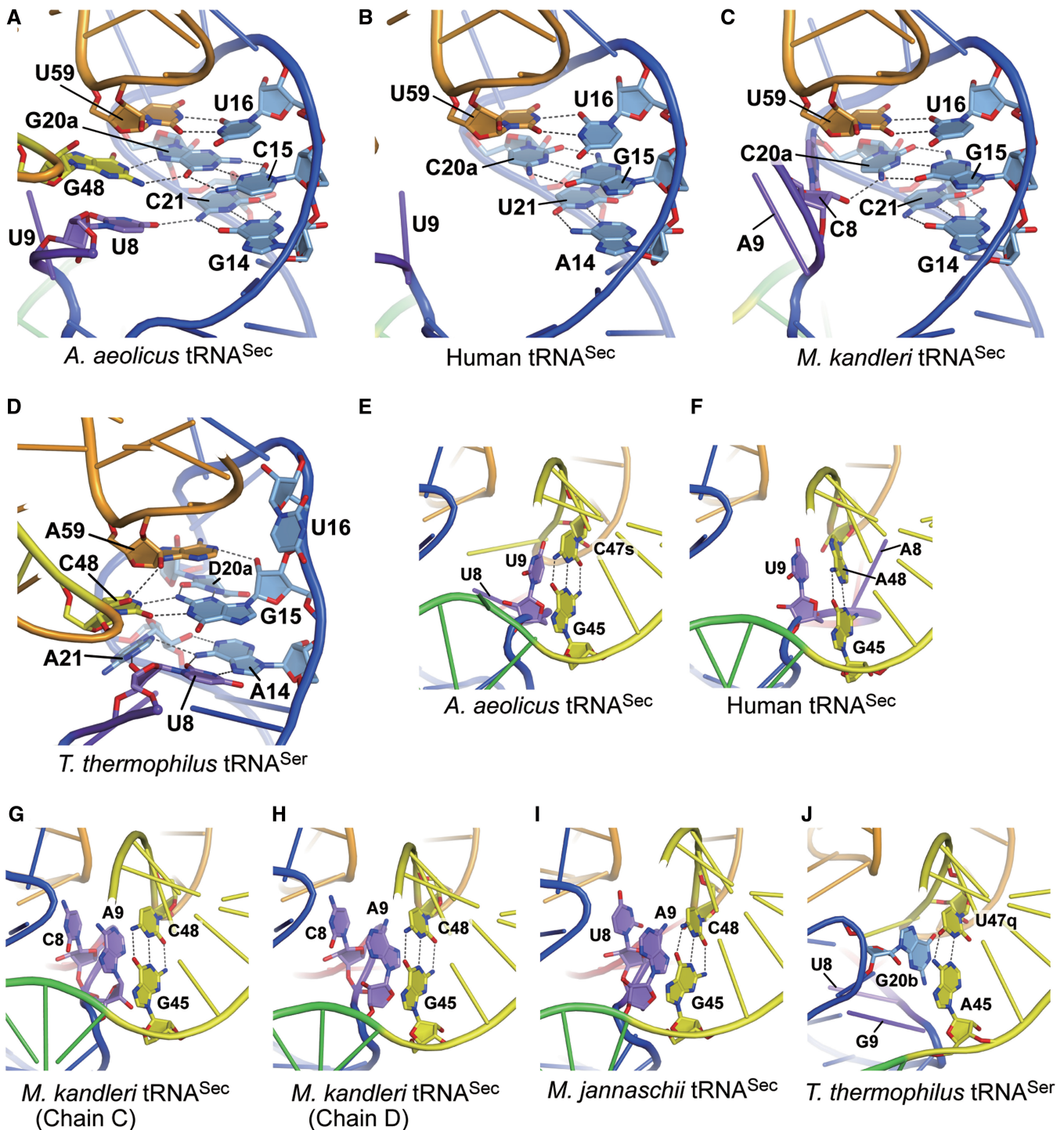
Figure 4. Tertiary interactions. (**A–D**) Close-up views of the tertiary interactions with the AD linker and the D arm. The linker nucleotides U8 and G48 in *A.aeolicus* tRNA^Sec interact with G14:C21 and C15:G20a in the D stem, respectively, to form unique base triples (A). In contrast, the D stem of human tRNA^Sec lacks the tertiary interaction (B), while C8 in *M. kandleri* tRNA^Sec interacts with the sixth D-stem base pair, G15:C21 (C). The N4 and O3′ atoms of C8 hydrogen bond with the O5′ and N4 atoms of C21, respectively. The nucleotides A14–A21 in *T. thermophilus* tRNA^Ser are included in the D loop, and form the canonical tertiary pairs U8:A14 and G15:C48 (D). Furthermore, U8:A14 interacts with A21, and G15:C48 interacts with D20a and A59, thus building a tertiary core. (**E–I**) The tertiary stacking of the linker nucleotide at position 9 on the first extra-arm stem for the *A. aeolicus* (E), human (F), *M. kandleri* (G and H) and *M. jannaschii* (I) tRNA^Secs. Two distinct A9 conformations are observed in the two *M. kandleri* tRNA^Sec molecules in the co-crystal with PSTK [PDB ID: 3ADD (11)]. The asymmetric unit contains two tRNA^Sec molecules (chains C and D) and one PSTK dimer, and the A9s in chains C and D adopt different ribose puckering modes, C3′-endo and C2′-endo, respectively (G and H). The C2′-endo puckering is assumed by the U9s of the *A. aeolicus* (E) and human (F) tRNA^Secs. On the other hand, the asymmetric unit of the *M. jannaschii* tRNA^Sec•PSTK co-crystal contains one tRNA^Sec molecule and one-half of a PSTK dimer [PDB ID: 3AM1 (14)], and the A9 ribose puckering is C2′-endo (I). C8 and U8 of the *M. kandleri* and *M. jannaschii* tRNA^Secs, respectively, are further stacked on A9. (**J**) The tertiary stacking in *T. thermophilus* tRNA^Ser. The D-loop nucleotide G20b is stacked on the first base pair of the extra-arm stem.

(Figure 4G and H). A9 in chain D has the same C2′-endo ribose puckering and base orientation as those of the U9s in the *A. aeolicus* and human tRNA^{Sec}s, while the A9 in chain C has the C3′-endo puckering and a different base
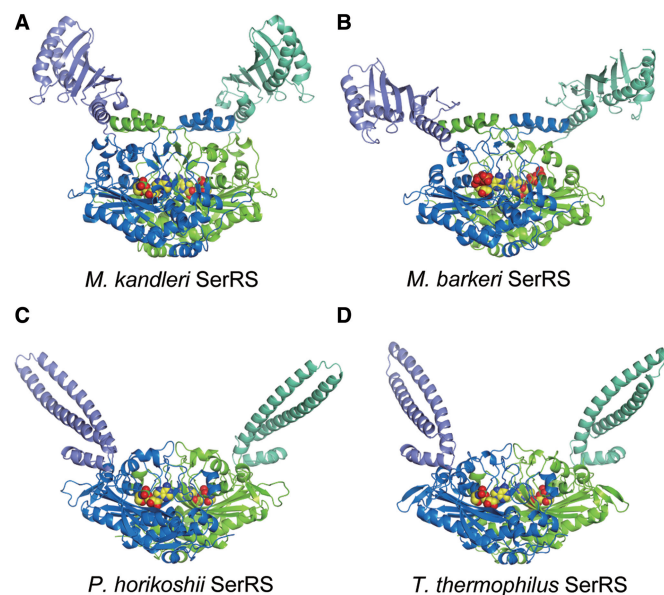
orientation. On the other hand, both A9s exhibit the C2′-endo puckering in the two molecules of tRNA^{Sec} from another archaeon, *Methanocaldococcus jannaschii* in complex with the PSTK dimer [PDB ID: 3AM1 (14)] (Figure 4I). The corresponding base stacking is also observed in tRNA^{Ser}. The D-loop nucleotide G20b is stacked on the first extra-stem base pair of *T. thermophilus* tRNA^{Ser} (Figure 4J), which results in essentially the same extra-arm orientation between tRNA^{Sec} and tRNA^{Ser}.

Regardless of these interior differences in the secondary and tertiary structures, the overall exterior structure of the bacterial tRNA^{Sec} is similar to those of the eukaryal/archaeal tRNA^{Sec}s (Figure 3A–C and E–G). This is due to the conservation of the D-arm conformation, the D-loop•T-loop interaction, the total length of the acceptor-T arm and the orientation of the long extra arm. It is surprising that the distinct $8+5$ and $9+4$ secondary structures result in the same exterior structure, while the total number of base pairs in the acceptor-T arm is the same (13 bp). The difference in the boundary between the acceptor and T arms is compensated by the linker nucleotides, U8 and G48, which are involved in the unique base triples, G14:C21:U8 and C15:G20a:G48, in the bacterial tRNA^{Sec}.

Figure 5. Structures of SerRSs. Ribbon models of SerRS (dimer), colored as in Figure 1E. The structures of the SerRSs from the methanogenic archaea *M. kandleri* (**A**) and *M. barkeri* (**B**) [PDB ID: 2CJA (19)] are atypical, while those of the SerRSs from the archaeon *Pyrococcus horikoshii* (**C**) [PDB ID: 2DQ0 (16)] and the bacterium *T. thermophilus* (**D**) [PDB ID: 1SET (27)] are universal. The present *M. kandleri* SerRS structure (A) is that in the SerRS•tRNA^{Sec} complex, while the others are the tRNA-free structures (B–C). The sphere models represent the seryl-adenylate intermediate analog Ser-SA (A, C and D) and ATP (B). In the tRNA-free structure of *M. barkeri* SerRS (B), the N-terminal domains are partially disordered, and the N-terminal-domain orientation differs significantly from that of the present SerRS•tRNA^{Sec} complex structure (A). The N-terminal domains of the universal SerRSs have a long coiled-coil, which is responsible for tRNA binding (C and D).

Table 2. The steady-state kinetics of aminoacylation

SerRS	tRNA^{Sec}	K_M (μM)	k_{cat} (s^{-1})	k_{cat}/K_M (s^{-1}μM^{-1})
M. kandleri	*M. kandleri*	0.57 ± 0.20	0.30 ± 0.10	0.77 ± 0.34
M. kandleri	*A. aeolicus*	109 ± 15	0.43 ± 0.05	0.0040 ± 0.00004
A. aeolicus	*M. kandleri*	0.52 ± 0.18	0.053 ± 0.009	0.19 ± 0.09
A. aeolicus	*A. aeolicus*	3.6 ± 0.5	0.42 ± 0.02	0.13 ± 0.02

The K_M and k_{cat} values of the wild-type *M.kandleri* and *A.aeolicus* SerRSs were measured.
Each experiment was performed 3–6 times, and the values were averaged.
The SEM values are shown as '±'.

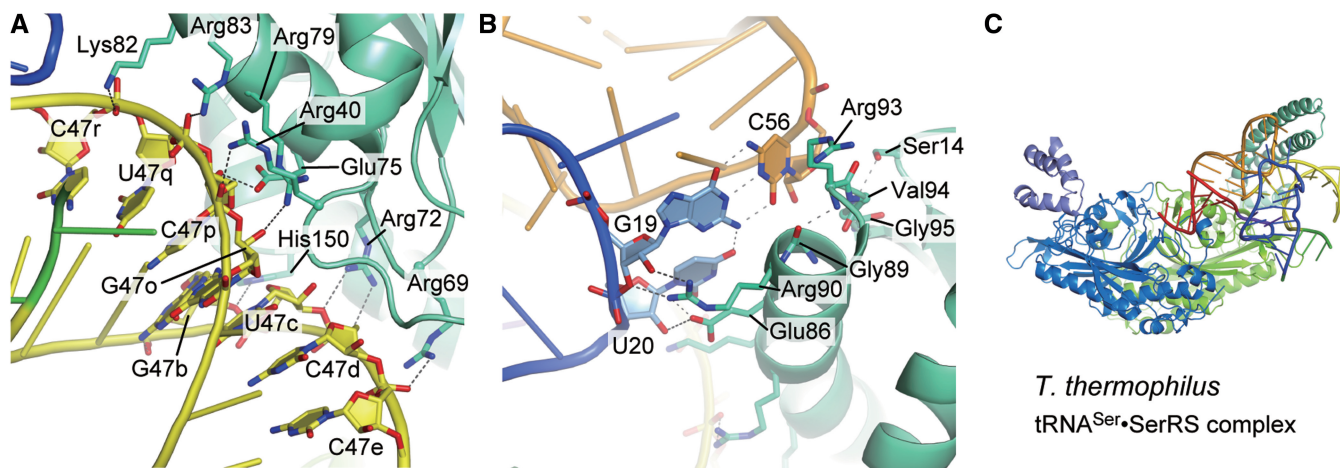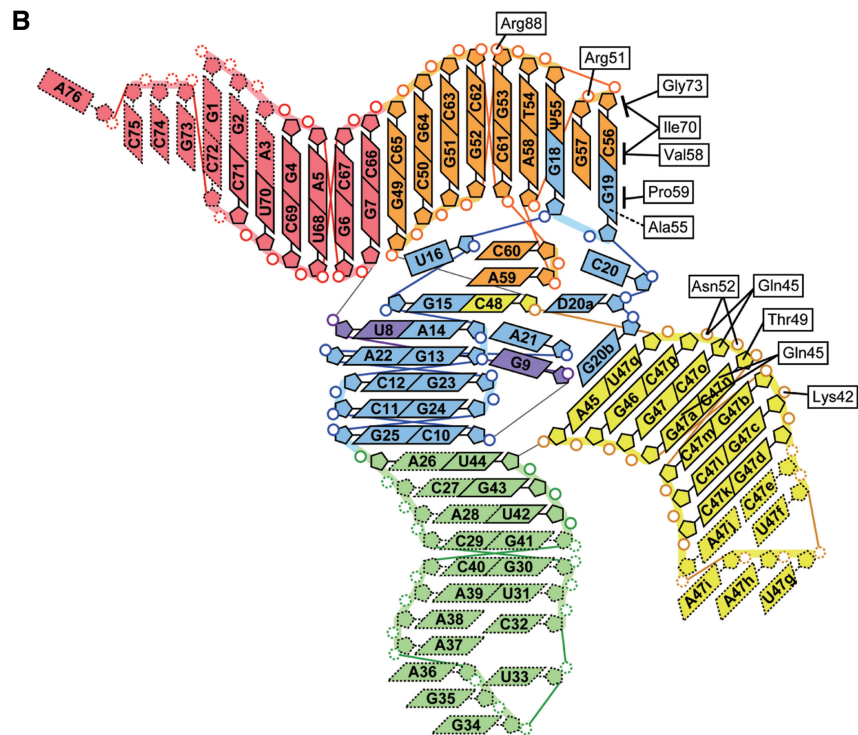**Figure 6.** Interactions between tRNA^{Sec} and SerRS. (**A** and **B**) Close-up views of the interaction between *A. aeolicus* tRNA^{Sec} and *M. kandleri* SerRS. The SerRS residues that interact with tRNA^{Sec} are represented by stick models. Possible hydrogen bonds are depicted as dashed lines. (**C**) An overall view of the *T. thermophilus* tRNA^{Ser}•SerRS complex. In the absence of the tRNA^{Ser} interaction, the coiled-coil is disordered.
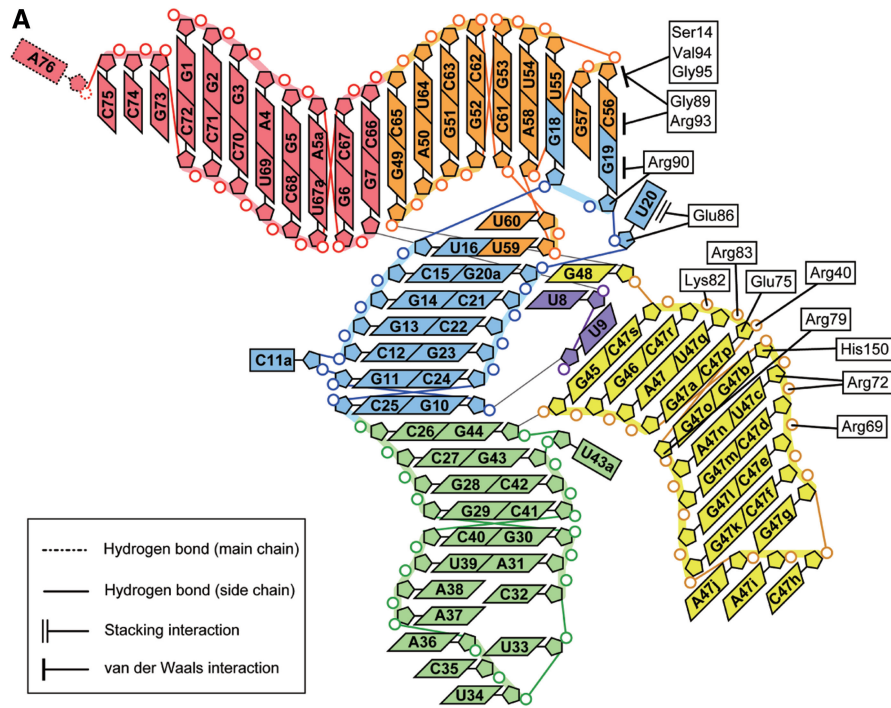
Figure 7. Comparison with tRNA^Ser and SerRS interaction. A diagram representing the tRNA^Sec•SerRS interactions observed in the present complex structure (**A**), and that representing the interactions between tRNA^Ser and the SerRS N-terminal domain in the *T. thermophilus* tRNA^Ser•SerRS complex [PDB ID: 1SER (9)] (**B**). In both of the complexes, the SerRS N-terminal domain interacts with the extra-arm stem and the outer corner of the tRNA.

These two unique base triples in the bacterial tRNA^{Sec} occupy the positions corresponding to the U8:A14 and R15:Y48 tertiary base pairs, conserved in the canonical tRNAs (Figure 4D). Here, R and Y denote G/A and C/U, respectively. In the canonical tRNAs, these tertiary base pairs form the tight 'tertiary core', with additional non-conserved base triples in the D stem, such as 45:10:25, 12:23:9 and 13:22:46 (24,25), or 12:23:9 in the case of a long extra arm (9). In contrast, the eukaryal tRNA^{Sec} completely lacks the corresponding interaction, and has a cavity instead of the tertiary core (10) (Figure 3J). On the other hand, the ribose and base moieties of C8 in the archaeal tRNA^{Sec} interact with the base and phosphate moieties of C20a, respectively (11) (Figure 4C), thus generating an incomplete core (Figure 3K). Along with the shift of the acceptor-T boundary from the 9 + 4 to 8 + 5 secondary structure, the bacterial tRNA^{Sec} generates the tertiary core, without any alterations in the overall exterior structure. The tertiary core reinforces the bacterial tRNA^{Sec} conformation, although its contribution is relatively weak, as compared with those observed in the canonical tRNAs.

Structure of *M. kandleri* SerRS

The *M. kandleri* SerRS, used for co-crystallization with *A. aeolicus* tRNA^{Sec}, is an atypical SerRS unique to methanogenic archaea. The aminoacyl-tRNA synthetases are divided into two classes, classes I and II, based on the two structurally unrelated catalytic core domains (26), and both the typical and atypical SerRSs belong to class II. Similar to the reported *M. barkeri* SerRS structure (19), *M. kandleri* SerRS consists of an N-terminal domain (residues 1–167) and a C-terminal catalytic domain (residues 168–527) (Figure 5A and B). The globular N-terminal domain is composed of a six-stranded β sheet and four α helices, in contrast to the coiled-coil N-terminal domain of the typical SerRSs (15,16,27) (Figure 5C and D). The SerRS homodimer is formed by inter-subunit interactions between the C-terminal catalytic domains.

Interaction of *M. kandleri* SerRS with *A. aeolicus* tRNA^{Sec}

Methanopyrus kandleri SerRS exhibited serine-ligation activity toward *A. aeolicus* tRNA^{Sec} *in vitro*, although the activity was lower than that toward *M. kandleri* tRNA^{Sec} (Figure 2 and Table 2). One SerRS homodimer binds two tRNA^{Sec} molecules. The N-terminal domain of SerRS interacts with the extra stem and the D and T loops of tRNA^{Sec} (Figures 6A and B, and 7A). The acceptor and anticodon arms do not interact with SerRS. The backbone of the second to eighth base pairs of the extra stem forms polar interactions with the SerRS residues (Figure 6A). The side chains of Arg40, Arg69, Arg72, Lys82 and Arg83 interact with the phosphate groups of C47p, C47e, C47d, C47r and U47q, respectively. The side chains of Arg72, Glu75 and His150 interact with the ribose moieties of C47d, C47p and G47b, respectively. The Arg76 side chain interacts with the ribose moieties of two nucleotides, C47o and C47p. The U20:G19:C56

base triple in the D-loop•T-loop interface interacts with SerRS (Figure 6B). The side chains of Glu86 and Arg90 interact with the ribose moieties of U20 and G19, respectively. Ser14, Gly89, Arg93, Val94 and Gly95 form van-der-Waals interactions with the base and ribose moieties of C56.

The K_M value of *M. kandleri* SerRS for *A. aeolicus* tRNA^{Sec} is much higher than that for *M. kandleri* tRNA^{Sec} (Table 2). Interestingly, the K_M value of *A. aeolicus* SerRS for *A. aeolicus* tRNA^{Sec} is also higher than that for *M. kandleri* tRNA^{Sec} (Table 2), suggesting that the affinity of the bacterial tRNA^{Sec} for SerRS is lower, as compared with that of the archaeal tRNA^{Sec}.

In the crystal structure, SerRS interacts with the extra stem and the outer corner of tRNA^{Sec} via its N-terminal domain, while the acceptor arm lacks interactions with SerRS. Therefore, this complex might be assumed to represent the pre-binding state of SerRS and tRNA^{Sec}, where only the N-terminal domain binds to tRNA^{Sec}. These tRNA–SerRS interactions are homologous to those between the N-terminal domain of the common type of SerRS and tRNA^{Ser} observed in the *T. thermophilus* SerRS•tRNA^{Ser} complex structure (9) (Figures 6C and 7B).

The unique secondary and tertiary structures of tRNA^{Sec} are responsible for its specific interactions with PSTK, SepSecS, SelA and EF-Sec. However, tRNA^{Sec} must also interact with SerRS to receive serine, and it has a long extra arm to mimic tRNA^{Ser}. The long extra arm of tRNA^{Ser} and tRNA^{Sec} is the determinant element for the SerRS interaction (9,28). Furthermore, the extra arm orientation of tRNA^{Sec} is adjusted to resemble that of tRNA^{Ser}, by the stacking interaction on the first extra-stem base pair by the nucleotides at positions 9 and 20b of tRNA^{Sec} and tRNA^{Ser}, respectively. On the other hand, the length of the acceptor stem is not important for SerRS (29,30), owing to the flexibility between its N- and C-terminal domains. The present complex structure indicated that tRNA^{Sec} is recognized by SerRS in the same manner as tRNA^{Ser}, and is thereby distinguished from the other tRNAs. The conformational flexibility between the N- and C-terminal domains may allow tRNA^{Sec} to retain the specific interaction between its extra arm and the SerRS N-terminal domain, when its 3′-terminal CCA region enters the SerRS catalytic site.

REFERENCES

1. Böck,A., Forchhammer,K., Heider,J., Leinfelder,W., Sawers,G., Veprek,B. and Zinoni,F. (1991) Selenocysteine: the 21st amino acid. *Mol. Microbiol.*, **5**, 515–520.
2. Leinfelder,W., Zehelein,E., Mandrand-Berthelot,M.A. and Böck,A. (1988) Gene for a novel tRNA species that accepts L-serine and cotranslationally inserts selenocysteine. *Nature*, **331**, 723–725.
3. Baron,C., Sturchler,C., Wu,X.Q., Gross,H.J., Krol,A. and Böck,A. (1994) Eukaryotic selenocysteine inserting tRNA species support selenoprotein synthesis in *Escherichia coli*. *Nucleic Acids Res.*, **22**, 2228–2233.
4. Abe,T., Ikemura,T., Sugahara,J., Kanai,A., Ohara,Y., Uehara,H., Kinouchi,M., Kanaya,S., Yamada,Y., Muto,A. *et al.* (2011) tRNADB-CE 2011: tRNA gene database curated manually by experts. *Nucleic Acids Res.*, **39**, D210–D213.
5. Sturchler,C., Westhof,E., Carbon,P. and Krol,A. (1993) Unique secondary and tertiary structural features of the eucaryotic selenocysteine tRNA^{Sec}. *Nucleic Acids Res.*, **21**, 1073–1079.
6. Yuan,J., Palioura,S., Salazar,J.C., Su,D., O'Donoghue,P., Hohn,M.J., Cardoso,A.M., Whitman,W.B. and Söll,D. (2006) RNA-dependent conversion of phosphoserine forms selenocysteine in eukaryotes and archaea. *Proc. Natl Acad. Sci. USA*, **103**, 18923–18927.
7. Xu,X.M., Carlson,B.A., Mix,H., Zhang,Y., Saira,K., Glass,R.S., Berry,M.J., Gladyshev,V.N. and Hatfield,D.L. (2007) Biosynthesis of selenocysteine on its tRNA in eukaryotes. *PLoS Biol.*, **5**, e4.
8. Forchhammer,K. and Böck,A. (1991) Selenocysteine synthase from *Escherichia coli*. Analysis of the reaction sequence. *J. Biol. Chem.*, **266**, 6324–6328.
9. Biou,V., Yaremchuk,A., Tukalo,M. and Cusack,S. (1994) The 2.9 Å crystal structure of *T. thermophilus* seryl-tRNA synthetase complexed with tRNA^{Ser}. *Science*, **263**, 1404–1410.
10. Itoh,Y., Chiba,S., Sekine,S. and Yokoyama,S. (2009) Crystal structure of human selenocysteine tRNA. *Nucleic Acids Res.*, **37**, 6259–6268.
11. Chiba,S., Itoh,Y., Sekine,S. and Yokoyama,S. (2010) Structural basis for the major role of *O*-phosphoseryl-tRNA kinase in the UGA-specific encoding of selenocysteine. *Mol. Cell*, **39**, 410–420.
12. Palioura,S., Sherrer,R.L., Steitz,T.A., Söll,D. and Simonovic,M. (2009) The human SepSecS-tRNA^{Sec} complex reveals the mechanism of selenocysteine formation. *Science*, **325**, 321–325.
13. Ganichkin,O.M., Anedchenko,E.A. and Wahl,M.C. (2011) Crystal structure analysis reveals functional flexibility in the selenocysteine-specific tRNA from mouse. *PLoS One*, **6**, e20032.
14. Sherrer,R.L., Araiso,Y., Aldag,C., Ishitani,R., Ho,J.M., Söll,D. and Nureki,O. (2011) C-terminal domain of archaeal *O*-phosphoseryl-tRNA kinase displays large-scale motion to bind the 7-bp D-stem of archaeal tRNASec. *Nucleic Acids Res.*, **39**, 1034–1041.
15. Cusack,S., Berthet-Colominas,C., Hartlein,M., Nassar,N. and Leberman,R. (1990) A second class of synthetase structure revealed by X-ray analysis of *Escherichia coli* seryl-tRNA synthetase at 2.5 Å. *Nature*, **347**, 249–255.
16. Itoh,Y., Sekine,S., Kuroishi,C., Terada,T., Shirouzu,M., Kuramitsu,S. and Yokoyama,S. (2008) Crystallographic and mutational studies of seryl-tRNA synthetase from the archaeon *Pyrococcus horikoshii*. *RNA Biol.*, **5**, 169–177.
17. Itoh,Y., Sekine,S. and Yokoyama,S. (2012) Crystallization and preliminary X-ray crystallographic analysis of bacterial tRNA^{Sec} in complex with seryl-tRNA synthetase. *Acta Crystallogr. Sect. F Struct. Biol. Cryst. Commun.*, **68**, 678–682.
18. Fukunaga,R. and Yokoyama,S. (2007) Structural insights into the first step of RNA-dependent cysteine biosynthesis in archaea. *Nat. Struct. Mol. Biol.*, **14**, 272–279.
19. Bilokapic,S., Maier,T., Ahel,D., Gruic-Sovulj,I., Söll,D., Weygand-Durasevic,I. and Ban,N. (2006) Structure of the unusual seryl-tRNA synthetase reveals a distinct zinc-dependent mode of substrate recognition. *EMBO J.*, **25**, 2498–2509.
20. Laskowski,R.A., MacArthur,M.W., Moss,D.S. and Thornton,J.M. (1993) PROCHECK: a program to check the stereochemical quality of protein structures. *J. Appl. Cryst.*, **26**, 283–291.
21. Adams,P.D., Pannu,N.S., Read,R.J. and Brunger,A.T. (1997) Cross-validated maximum likelihood enhances crystallographic simulated annealing refinement. *Proc. Natl Acad. Sci. USA*, **94**, 5018–5023.
22. Adams,P.D., Afonine,P.V., Bunkóczi,G., Chen,V.B., Davis,I.W., Echols,N., Headd,J.J., Hung,L.W., Kapral,G.J., Grosse-Kunstleve,R.W. *et al.* (2010) PHENIX: a comprehensive Python-based system for macromolecular structure solution. *Acta Crystallogr. D Biol. Crystallogr.*, **66**, 213–221.
23. Emsley,P. and Cowtan,K. (2004) Coot: model-building tools for molecular graphics. *Acta Crystallogr. D Biol. Crystallogr.*, **60**, 2126–2132.
24. Robertus,J.D., Ladner,J.E., Finch,J.T., Rhodes,D., Brown,R.S., Clark,B.F. and Klug,A. (1974) Structure of yeast phenylalanine tRNA at 3 Å resolution. *Nature*, **250**, 546–551.
25. Kim,S.H., Suddath,F.L., Quigley,G.J., McPherson,A., Sussman,J.L., Wang,A.H., Seeman,N.C. and Rich,A. (1974) Three-dimensional tertiary structure of yeast phenylalanine transfer RNA. *Science*, **185**, 435–440.
26. Eriani,G., Delarue,M., Poch,O., Gangloff,J. and Moras,D. (1990) Partition of tRNA synthetases into two classes based on mutually exclusive sets of sequence motifs. *Nature*, **347**, 203–206.
27. Belrhali,H., Yaremchuk,A., Tukalo,M., Larsen,K., Berthet-Colominas,C., Leberman,R., Beijer,B., Sproat,B., Als-Nielsen,J., Grübel,G. *et al.* (1994) Crystal structures at 2.5 angstrom resolution of seryl-tRNA synthetase complexed with two analogs of seryl adenylate. *Science*, **263**, 1432–1436.
28. Asahara,H., Himeno,H., Tamura,K., Nameki,N., Hasegawa,T. and Shimizu,M. (1994) *Escherichia coli* seryl-tRNA synthetase recognizes tRNA^{Ser} by its characteristic tertiary structure. *J. Mol. Biol.*, **236**, 738–748.
29. Baron,C. and Böck,A. (1991) The length of the aminoacyl-acceptor stem of the selenocysteine-specific tRNA^{Sec} of *Escherichia coli* is the determinant for binding to elongation factors SELB or Tu. *J. Biol. Chem.*, **266**, 20375–20379.
30. Sherrer,R.L., Ho,J.M. and Söll,D. (2008) Divergence of selenocysteine tRNA recognition by archaeal and eukaryotic *O*-phosphoseryl-tRNA^{Sec} kinase. *Nucleic Acids Res.*, **36**, 1871–1880.